IEEE Access
Multidisciplinary ⋮ Rapid Review ⋮ Open Access Journal

Received July 18, 2021, accepted July 31, 2021, date of publication August 3, 2021, date of current version August 9, 2021.

Digital Object Identifier 10.1109/ACCESS.2021.3102182

Evaluation of a Novel Spectral Pair of a Chirp FBG Embedded in a Cantilever Beam for Simultaneous Temperature and Transverse Forces Measurement

ABDULFATAH A. G. ABUSHAGUR[1,2], NORHANA ARSAD[1], (Senior Member, IEEE), MOHAMED M. ELGAUD[1,3], AND AHMAD ASHRIF A. BAKAR[1], (Senior Member, IEEE)

[1]Center of Advanced Electrical and Communication Engineering (PAKET), Faculty of Engineering and Built Environmental, Universiti Kebangsaan Malaysia (UKM), Bangi, Selangor 43600, Malaysia
[2]Department of Electrical and Electronic Engineering, Faculty of Engineering, University of Gharyan, Gharyan 21841, Libya
[3]College of Electrical and Electronics Technology (CEET), Benghazi 16063, Libya

Corresponding authors: Abdulfatah A. G. Abushagur (abushagur@ukm.edu.my) and Norhana Arsad (noa@ukm.edu.my)

This work was supported in part by the Universiti Kebangsaan Malaysia through the Human Capital under Grant MI-2020-001, and in part by the Research University under Grant IF0419IF1082.

ABSTRACT An evaluation of a novel spectrum features combining the distant longer and shorter wavelengths of a single chirped fiber Bragg grating (CFBG) for temperature and transverse forces discrimination is experimentally demonstrated. The shift of the two distant wavelengths' pair is compared with the conventional pair combining the bandwidth modulation and center wavelength shift. The CFBG sensor is simply bonded to a cantilever beam and subjected to transverse loading (four times) and a heating-cooling cycle. The transverse forces calibration results show a repeatability of 3.9 pm and 1.7 pm for the bandwidth's and center wavelength's responses, respectively, while the distant wavelengths' show a repeatability of 2.37 pm and 3.01 pm, respectively. The cantilever CFBG sensor exhibits high correlation coefficients of 0.9 between the two heating and cooling data sets, except for the bandwidth, which only had a lower coefficient of 0.75. The linear model of both pairs for calculating temperature and transverse forces can provide an accurate estimate, with the longer-shorter wavelengths' pair having an advantage over the pair of the bandwidth-centre-wavelength. The study has demonstrated the feasibility of the method proposed by our group in a previous work, by which three physical quantities can be measured with a single custom FBG.

INDEX TERMS Fiber Bragg grating, chirp, strain and temperature discrimination, force sensors, temperature sensor.

I. INTRODUCTION

Cross sensitivity of the central resonance wavelength shift of fiber Bragg grating (FBG) between the temperature and the mechanical strain is the main challenge in many applications. Eliminating the effect of either one, the temperature or the strain, were the approaches adopted for measurement for more than a decade. The situation in which more than one FBG sensor are required to be employed to achieve the elimination tactic. This usually leads to complexities in sensor packaging and data acquisition. Therefore, it is desired to measure either one independently using only a single FBG.

The associate editor coordinating the review of this manuscript and approving it for publication was Muguang Wang.

The reflectivity spectrum of the FBG besides the Bragg central resonance wavelength (CRW) has several attributes, such as the spectral width (FWHM), intensity [1], sidelobe power [2], and peak reflectivity. Researchers have made numerous attempts to address the cross-sensitivity issue by employing some pairs of these spectrum attributes for discrimination purposes [3]–[6].

When the spectrum's pair FWHM with CRW is used, the most exciting and reliable, reproducible FBG sensor is created. Researchers in [6]–[9] must manipulate the mechanism of the FBG sensor housing prior to experimentation in order to induce a non-uniform strain (spatial gradient) along the FBG under longitudinal tension. This enables them to demodulate the FWHM and the CRW in order to distinguish

between two metrics of interest (e.g., water level and temperature). There are, however, several applications where FBGs are surface mounted/embedded on flexible smart structures where loads can be applied axially and transversely, inducing both uniform and non-uniform strains along with the structure containing the FBG sensor [9]–[13]. In such cases, it is preferable to monitor both strain and temperature at the same time. To accomplish this, the traditional FWHM&CRW pair is insufficient; instead, an additional spectrum feature with a different sensitivity is required.

Recently, in [14], our group proposed a new pair of spectral features for distinguishing temperature and transverse forces by combining the distant wavelengths longer and shorter resonances (LRW&SRW). The use of three spectrum attributes, such as LRW, SRW, and CRW, can be extremely beneficial in discriminating between two forces and temperature, for example, in the extensive research that has recently been conducted on the tapered FBG (TFBG) [7]–[12].

A single linearly chirped FBG (CFBG) sensor is used in this work. The grating period along its sensing element (z-axis of the fiber) are monotonically increased during fabrication, which gradually localizes the wavelengths. The farthest wavelengths of the CFBG are indicated throughout this paper as longer LRW and shorter wavelengths SRW.

This study aims to investigate the response of the two reflection spectra pairs of the CFBG (conventional pair FWHM&CRW and proposed pair LRW&SRW) to the transverse forces and temperature and perform a feasibility assessment of the proposed spectral pair for simultaneous temperature and transverse forces measurement.

The paper is organized as follows, theory and sensing principle in Section II, Section III discusses the experimental calibration process, results, and simultaneous measurement in Section IV, and concludes in Section V.

II. THEORY AND SENSING PRINCIPLE

The proposed force and temperature sensing module are based on a metal ruler (indicated as a simple beam) integrated with a single CFBG. A slot structure (square groove) is made along the top surface of the beam to a depth of y_d for the CFBG to conveniently lies down. The CFBG is bonded in the groove such that the shorter wavelength region (λ_{SRW}) is proximal to the fixed-end of the beam. The sensor module is then subjected to both transverse forces (F_y) and temperature changes (ΔT). Figure 1 shows the schematic diagram of the sensor module, the insets illustrate the induced bending moment and sideview of the beam and sensor being buried in the groove, respectively.

The F_y are applied at the beam's tip (free end), which causes the beam to bend. According to Bernoulli's beam theory, bending moment (M_x) to resist the bending force would be induced (see Figure 1), where the beam bends along the negative y-axis.

The spatial gradient strain along the beam's surface is linearly dependent on the bending moment, and therefore, it is localized and proportional to the F_y applied at the beam's tip. The local strain can be calculated according to the beam theory as follow,

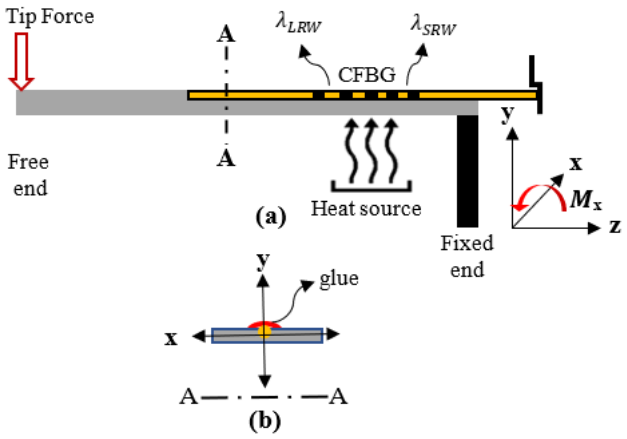

FIGURE 1. (a) A schematic of one-axis force and temperature sensing cantilever beam module subjected to transverse force and temperature changes with an inset illustrating the coordinate system including bending moment, (b) Cross-sectional view of AA, the grey substrate and the orange wire represent the beam and fiber optic respectively, whereas the red layer represents the glue.

$$\varepsilon(z) = \frac{M_x(z)\, y_t}{E_b I_b} = \frac{F_y z (y_t - y_d)}{E_b I_b} \tag{1}$$

where E_b is Young's modulus of the beam, I_b is the second moment of the beam, which can be defined as $I_b = \frac{bh^3}{12}$ where b and h are the breadth and thickness of the beam, y_t is the distance from the neutral axis to the beam's surface, and z is the distance between the fixed-point and the local segment of the CFBG. The sensitivity of the CFBG is governed mainly by the nature of the strain-induced to the beam on which fiber embedded within. Spatial uniform strain and gradient strain would be induced when fiber is exposed to both ΔT and F_y, respectively. In the following subsections the relationship between ΔT and F_y to the responses of the four spectrum features will be discussed.

Figure 2 shows the two pairs of the CFBG's spectrum features at room temperature.

A. THE RESPONSES OF THE LRW AND SRW

In this subsection, the ΔT and F_y calculation algorithms as a function of the first pair of the CFBG's spectrum parameters LRW and SRW is discussed. Figure 2 shows the spectrum of the CFBG, the amount of shift in both wavelengths the longer $\Delta\lambda_{LRW}$ and shorter $\Delta\lambda_{SRW}$ due to strain and temperature variations is given by;

$$\Delta\lambda_{LRW} = k_{\varepsilon lw}\mathcal{E}_{LRW} + k_T \Delta T \tag{2}$$

And

$$\Delta\lambda_{SRW} = k_{\varepsilon sw}\mathcal{E}_{SRW} + k_T \Delta T \tag{3}$$

where E_{LRW}, and E_{SRW} denote local strain at longer and shorter wavelengths, respectively, ΔT denotes the temperature change, $k_{\varepsilon lw,\varepsilon sw}$ and k_T denote the constant sensitivity

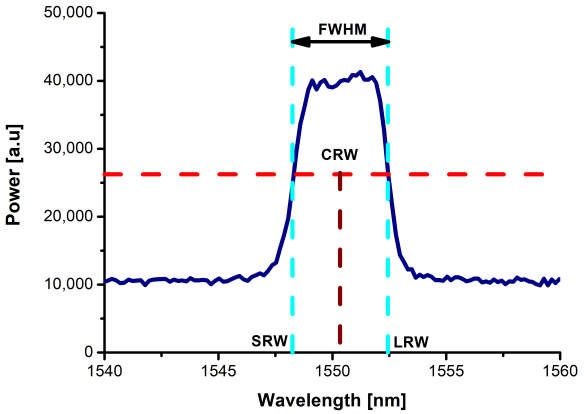

FIGURE 2. Reflection spectrum of the CFBG showing the two pairs of the spectrum features utilized in the two compared interrogation methods (FWHM&CRW, LRW&SRW).

ratio associated with strain and temperature, respectively. Substituting (1) in (2) and (3) we get,

$$\Delta\lambda_{LRW} = k_{\varepsilon lw}\frac{F_y Z_{LW}(y_t - y_d)}{E_b I_b} + k_T \Delta T \tag{4}$$

And

$$\Delta\lambda_{SRW} = k_{\varepsilon sw}\frac{F_y Z_{SW}(y_t - y_d)}{E_b I_b} + k_T \Delta T \tag{5}$$

where Z_{SW} and Z_{LW} are the distances from the fixed-end of the beam to the proximal and distal position edges of FBG sensor. Equations (4) and (5) can be expressed as follow;

$$\begin{aligned}\Delta\lambda_{LRW} &= k_{FLW}F_y + k_T\Delta T\\ \Delta\lambda_{SRW} &= k_{FSW}F_y + k_T\Delta T\end{aligned} \tag{6}$$

Here k_{FLW} and k_{FSW} are the proportionality constant representing the sensitivity ratio of LRW and SRW with respect to applied transverse force, respectively.

Then we can use matrix notation to map the cut-off wavelengths reading independently to force and temperature calculations as follow;

$$\begin{bmatrix} F_y & \Delta T \end{bmatrix}^T = K^{-1}\begin{bmatrix} \Delta\lambda_{LRW} & \Delta\lambda_{SRW} \end{bmatrix}^T \tag{7}$$

where K^{-1} is 2×2 inverse matrix of the transfer function with the coefficients obtained from the calibration.

B. BANDWIDTH FWHM AND CRW RESPONSES

This subsection discusses the conventional method which employs the bandwidth FWHM and CRW of the CFBG sensor. Since the strain-induced is gradient, the amount of shift of the CRW depends on the local strain at Z_{CRW} as;

$$\Delta\lambda_{CRW} = k_{\varepsilon crw}\frac{F_y Z_{CRW}\,(y_t - y_d)}{E_b I_b} \tag{8}$$

Here the $k_{\varepsilon crw}$ denotes the constant sensitivity ratio of the CRW associated with induced strain. Then the expression can be defined with respect to the applied force and temperature change as follows;

$$\Delta\lambda_{CRW} = k_{FCRW}F_y + k_T\Delta T \tag{9}$$

Here k_{FCRW}, k_T denote the sensitivity ratio of the CRW response to force applied and temperature change, respectively.

Bandwidth can be tuned only if spatial gradient strain is induced along the FBG, in other words, when both longer and shorter wavelengths respond with different sensitivity to the applied force, thus the signal of the bandwidth variation which is tuned by forces applied is given by;

$$\Delta FWHM_s = (\lambda_{LRW} - \lambda_{SRW}) + (\Delta\lambda_{LRW} - \Delta\lambda_{SRW}) \tag{10}$$

This equation can also be expressed further with respect to applied force as [13];

$$\begin{aligned}\Delta FWHM_s &= FWHM_r + \Delta FWHM_r\\ \Delta FWHM_r &= \Delta FWHM_s - FWHM_r = k_{F(fwhm)}F_y\end{aligned} \tag{11}$$

Here, $k_{F(fwhm)}$ denotes the sensitivity ratio of the bandwidth's reading signal. The temperature effect is eliminated as k_T for both $\Delta\lambda_{LRW}$ and $\Delta\lambda_{SRW}$ is equal. Combining equations (10) and (11), the matrix notation of the transfer function can be expressed as;

$$k = \begin{bmatrix} k_{F(fwhm)} & 0 \\ k_{FCRW} & k_T \end{bmatrix} \tag{12}$$

The TF and temperature, therefore, can be independently measured using the following linear model;

$$\begin{bmatrix} F_y & \Delta T \end{bmatrix}^T = K^{-1}\begin{bmatrix} \Delta FWHM_r & \Delta\lambda_{CRW} \end{bmatrix}^T \tag{13}$$

where K^{-1} is 2×2 inverse matrix of the transfer function to map from the CFBG (CRW shift and FWHM tunes) readings to the F_y and ΔT temperature.

III. EXPERIMENTS AND RESULTS

In this work, a single CFBG sensor with a length of 10 mm is used to measure transverse forces (tip force) and temperature simultaneously.

A. EXPERIMENTAL SETUP

The CFBG sensor is inserted into a longitudinal groove on top of the surface of a cantilever beam as showed in Figure 1(b). An adhesive of type LOCTITE 401 is used to bond the CFBG in the groove. The simplified schematic version of the experimental set up for calibrating and validating the sensor module is shown in Figure 3(a).

The CFBG sensor is illuminated by a superluminescent light-emitting diode (SLED) through a built-in optical circulator, the back-reflected light from the CFBG travel to the FBG interrogator IMON-256USB (Ibsen Photonics, Rytter-Marken 17, Denmark) in which transmission diffraction gratings disperse the incoming light to be eventually focused onto an array of photodiodes (pixels). The beam spot position is then connected to the optical wavelength and sent to a computer through a high-speed USB interface.

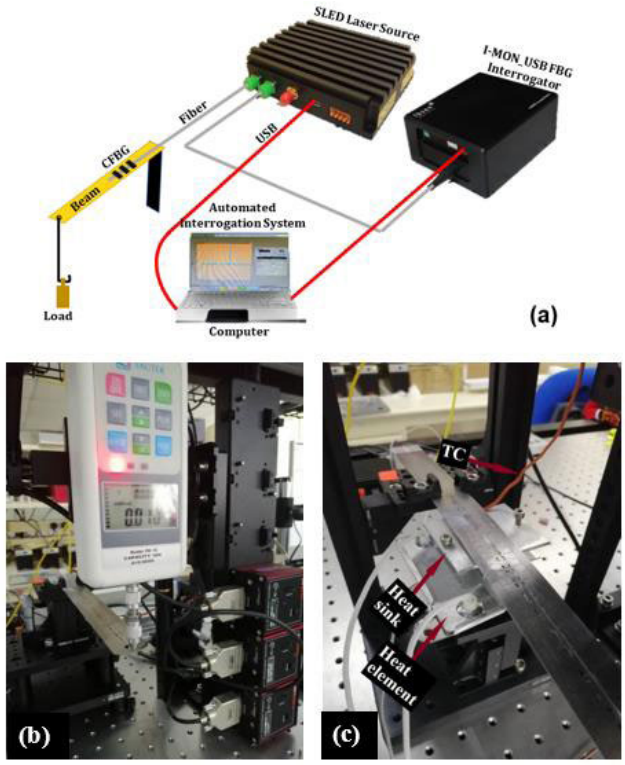

FIGURE 3. (a) Experimental setup schematically illustrating the most critical components of the system, (b) The beam incorporating CFBG subjected to the transversal forces by controlling the SAUTER force gauge, (c)The beam also subjected to the temperature variations through heat sink to which heat element is attached.

B. CALIBRATION PROCEDURES

The calibration procedure of the transverse forces is carried out using, a tri-axis motorized stages (x, y, and z) and a force-gauge (SAUTER GMBH) of type FH10 which can provide a maximum force of 10N with a resolution of 0.005N. The motorized stages are used to drive the force gauge within a limit of travel distance of 12mm. The SAUTER force-gauge is guided to be aligned vertically to the cantilever beam's tip (free end) as shown in Figure 3(b).

On the other hand, the calibration procedure of the temperature effect is conducted utilizing a thermocouple (TC), temperature controller, heat element, and a heat sink, as shown in Figure 3(c). The TC signal is acquired through a USB interface by using a DAQ module from National Instruments (NI-USB-DAQ6122).

The calibration procedure for both the transverse forces and temperature are carried out individually with an automated calibration system developed using the LABVIEW program. The LABVIEW program is developed with two algorithms that enabled a more precise analysis of the data in which signal processing is performed to calculate the four spectrum features: LRW, SRW, CRW, and FWHM. It is also worth mentioning that the FBG sensor was sampled in this work at a scan rate of 1 kHz due to the size of the program.

1) TRANSVERSE FORCES CALIBRATION RESULTS

The beam is fixed at one end while its other end subjected to the loads transversely. As shown in Figure 3(c), the forces applied at the free end of the beam are controlled by the automated system by controlling the motion of the vertical "z" motorized translation stage. The force-gauge pushes the beam downward at the beam's tip (bending) with an interval translation step of 0.5 mm, then drove back upward to straighten up the beam back with the same interval step. During the bending procedure the forces applied increase from 0 N to $\approx$ 0.85 N and then back to 0 N. This procedure is repeated four times at a constant temperature $\approx$ 25°C. Therefore, the data samples of the four subsets are collected and logged into a file for further analysis. Figure 4(a) and (b) illustrate the responses of the conventional method which is characterized by the spectrum parameters' pair of FWHM and CRW during beam's bending and straightening procedures.

The data points which are demonstrated in the two figures are the average values of the four experiments across the range of applied forces. Due to the CFBG sensor configuration, the bandwidth in Figure 4(a) is narrowed for every increase in applied force. Regression analysis is carried out to determine the standard residual error of the FWHM tuning which is shown in the inset. To compare how much data of bandwidth has been deviated compared to other wavelengths, we must consider the range of each response function, after which the residual error % with respect to the function range can be calculated as follows;

$$error\%\ (function\ range) = \frac{\max(|residual\ error|)}{function\ range} * 100 \tag{14}$$

Although the calculated percentage residual error of the FWHM with respect to its tuned range is found $\approx$12.7%, a high correlation between the two data sets is obvious. The behavior of the central resonance wavelength CRW is shown in Figure 4(b). It is noticeable that the data very reliable and correlate very well for increasing and decreasing applied forces. The error % with respect to its shift range is found only 0.9%.

The second pair of reflection spectrum parameters of the CFBG (proposed in our previous work [14]) which represented by LRW and SRW are illustrated in Figure 4(c) and (d). As we can see from both responses, the data points exhibited consistency and are highly correlated for both procedures. The insets in both figures illustrate the residual error of both wavelengths' responses to the transverse forces. The percentage residual error for both wavelengths is around 2% with respect to their shifts' range. It is noticeable that in the four calibration results, the data points during beam bending and straightening are offset, that is due to the force values applied with the same translation step interval in the two procedures (downward and upward) are not equal.

The regression statistics for the two spectrum pairs are summarized in the Table 1. The table illustrates the value and

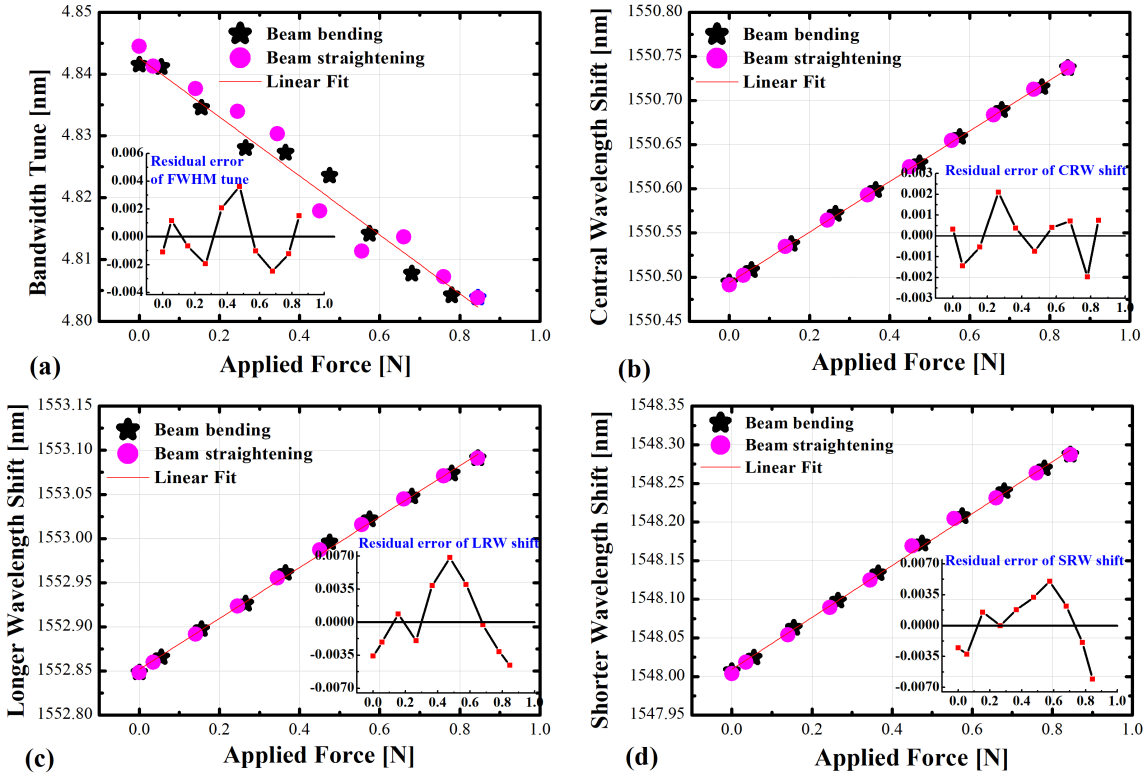

FIGURE 4. The response of the two pairs of the spectrum features to the applied forces (a) bandwidth of the CFBG, (b) the central resonance wavelength CRW, (c) the longer resonance wavelength LRW, (d) the shorter resonance wavelength SRW.

TABLE 1. Regression analysis summary of the transversal force calibration results.

	Intercept		Slope		Statistics
	Value	Standard Error	Value	Standard Error	Adj. R-Square
FWHM Tune	4.84259	0.00118	-0.0477	0.00233	0.97899
CRW Shift	1550.49	7.09E-4	0.28675	0.0014	0.99979
LRW Shift	1552.85	0.00227	0.28834	0.00447	0.99784
SRW Shift	1548.00929	0.00202	0.33602	0.00398	0.99874

TABLE 2. Regression statistics of temperature calibration results.

	Intercept		Slope		Statistics
	Value	Standard Error	Value	Standard Error	Adj. R-Square
FWHM Tune	4.84491	0.02345	0.00123	4.459E-4	0.484
CRW Shift	1550.13872	0.0242	0.01532	4.602E-4	0.994
LRW Shift	1552.51416	0.0382	0.01549	7.255E-4	0.985
SRW Shift	1547.66925	0.0256	0.01426	4.869E-4	0.992

standard error of the intercept and slope of each parameter as well as linear fit measure R^2.

2) TEMPERATURE VARIATIONS CALIBRATION RESULTS

The beam incorporating CFBG has been exposed to heating and cooling procedures using the heat sink as shown in figure 3(c).

Figure 5 (a) and (b) show the response of the FWHM&CRW's pair of the CFBG's spectrum as the temperature alternates up and down. Although the FWHM is not supposed to respond to temperature variations, the results in Figure 5(a) show that both procedures do respond. This can be attributed to the temperature distribution, which was spatially nonuniformly distributed along with the CFBG sensor, as a result of our work's improper heating system. Heat transfer through the beam takes time to distribute uniformly along the sensor segment. In contrast, the central resonance wavelength CRW exhibits a linear response in both temperature variation procedures, as shown in figure 5(b). Figures 5(a) and 5(b) include insets displaying the residual error of the FWHM and CRW responses to.

On the other hand, the response of the second spectrum pair features the LRW and SRW are illustrated in Figure 5(c) and 5(d), respectively. It is seen that the data points from both procedures are highly correlated and consistent. Regression statistics of the temperature calibration results for both pair of spectra are listed in Table 2.

From Table 1 and Table 2, the force and temperature calculation algorithms for both FWHM-CRW and LRW-SRW

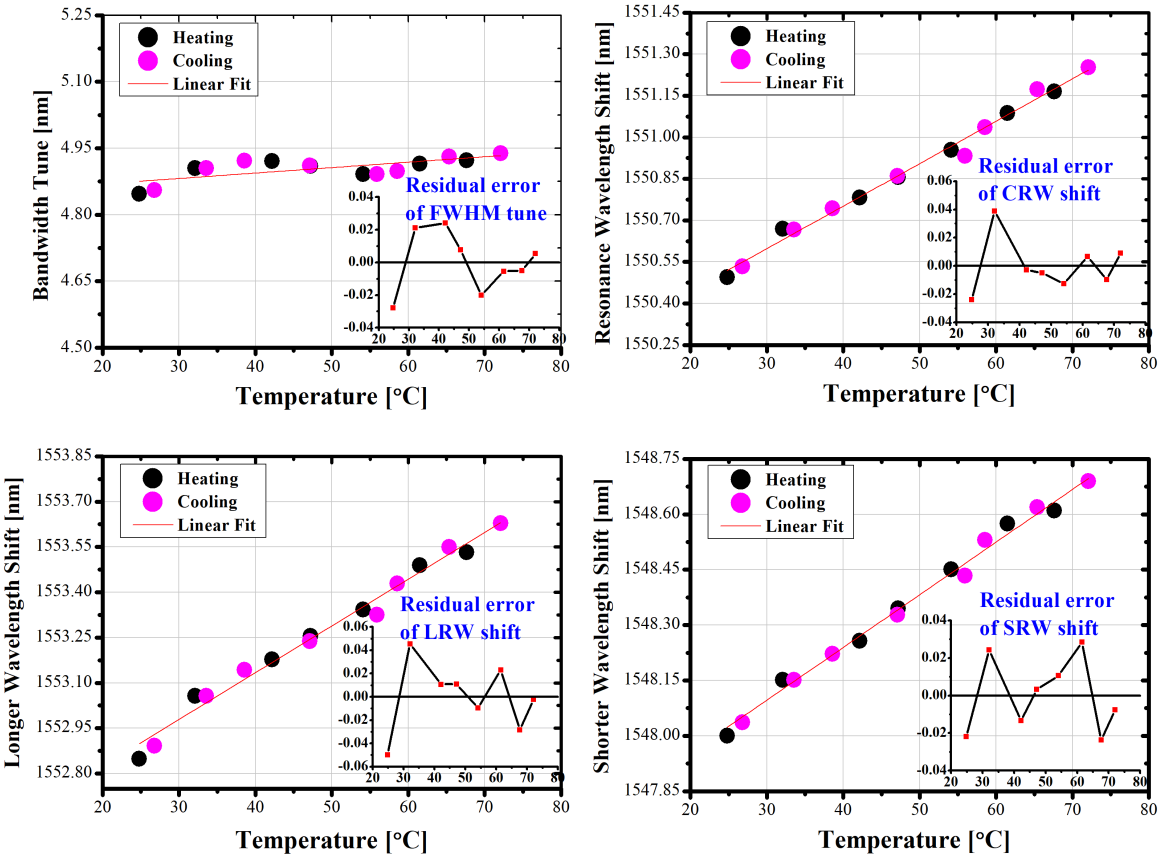

FIGURE 5. The response of the two CFBG's reflection spectrum pairs to temperature changes for both heating and cooling, (a) the FWHM tune, (b) The central wavelength CRW, (c) The longer wavelength LRW, (d) The shorter wavelength SRW.

pairs can be fully expressed respectively using the obtained constant coefficients as follow;

$$\begin{bmatrix} F_y & \Delta T \end{bmatrix}^T = \begin{bmatrix} -20.96 & 0 \\ 392.398 & 65.27 \end{bmatrix} \begin{bmatrix} \Delta BW_r \\ \Delta\lambda_{CRW} \end{bmatrix} \quad (15)$$

And

$$\begin{bmatrix} F_y & \Delta T \end{bmatrix}^T = \begin{bmatrix} -20.97 & 20.97 \\ 473.62 & -406.41 \end{bmatrix} \begin{bmatrix} \Delta\lambda_{LRW} \\ \Delta\lambda_{SRW} \end{bmatrix} \quad (16)$$

According to the results one can notice that the slopes of the LRW and SRW are different due to the transverse forces. On the contrary, they are equal with respect to the temperature effect. Thus, the method is able to distinguish between the two measurands.

C. VALIDATION

The following experiments are performed to validate whether the force and temperature calculation algorithms, using the constant sensitivity ratio obtained from calibration, provide reliable simultaneous measurement. Eventually, the comparison between the two methods is discussed to verify the new method previously proposed by our group.

The computational algorithms are injected into the LABVIEW program to simultaneously estimate the temperature ΔT and the transverse force F_y for both methods. The real time procedure of the experiment that we adopted is to increase the applied force and temperature simultaneously. Then we halt at a specific force value while keep increasing the temperature slightly. Due to the time for the heat it takes to transfer in the metal beam. We wait at least 5 minutes elapsed time after every increase in temperature.

Figures 6(a) and 6(b) show the simultaneous temperature and transverse forces measurement. The figures illustrate the temperature versus the applied forces for the actual and estimated values of both LRW&SRW and FWHM&CRW pairs, respectively. The actual temperature variations and applied forces are acquired from the TC and SAUTER force gauge, correspondingly. Figure 6(a) depicts the values of both the temperature and the transverse forces which are estimated by the LRW&SRW's pair method compared with the actual values. Meanwhile, in Figure 6 (b) the values of both temperature and forces which are estimated by the FWHM&CRW method are compared with the actual ones. For both spectral pairs methods as the temperature rises, it is observed that a reduction in the force estimations occurred at the three fixed values of applied forces. This may be attributed to the fact that the temperature is not yet distributed equally along with the CFBG sensor.

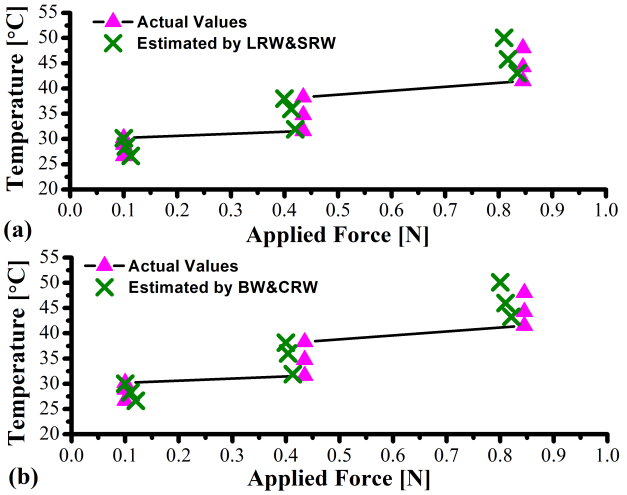

FIGURE 6. Actual values of temperature and applied transversal forces are compared with simultaneous estimated values of temperature changes and forces applied, (a) Utilizing LRW&SRW spectrum pair, (b) Utilizing FWHM&CRW spectrum pair.

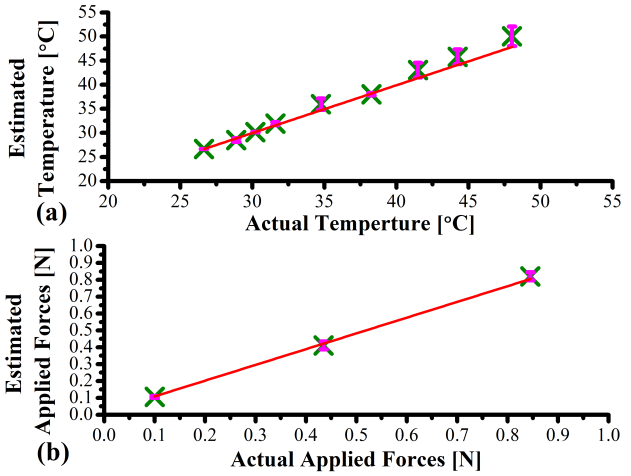

FIGURE 7. Linear fit of FWHM&CRW's response to (a) Temperature changes, and (b) Applied transversal forces.

Furthermore, it is seen that the estimated temperature's values slightly deviated from the actual ones for both methods. In our reading of the temperature, we rely on the TC. Hence the resulting errors may be due to the accuracy of the TC itself, or by referring to the Figure 3 (c), it is either due to the differences in the TC's and the CFBG sensor's position, or the contact force between the TC and the beam.

Figures 7(a) and 7(b) illustrate the estimated temperature and transverse forces versus their actual values, respectively. The figures also show the bar errors and the linear fitting results. It was evident that the FWHM&CRW pair can provide an accurate temperature and forces estimation with an RMS error of only 1.18°C and 0.027 N, respectively. In contrast to that, the other pair shown in Figure 8 (a) and (b) based on LRW&SRW can provide an even more accurate

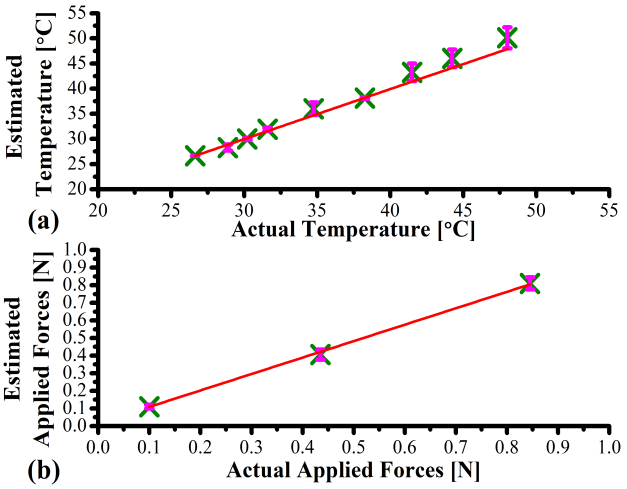

FIGURE 8. Linear fit of LRW&SRW's response to, (a) Temperature changes, and (b) Applied transversal forces.

TABLE 3. Summary of the calibration and validation results of both pair interrogation methods.

	Pair (method)	Repeatability /correlation	RMS error
F_y	FWHM&CRW	3.9 pm & 1.7 pm	0.027 N
	LRW&SRW	2.4 pm & 3.01 pm	0.02 N
Temperature	FWHM&CRW	0.754 & 0.995	1.2 °C
	LRW&SRW	0.988 & 0.993	1.08 °C

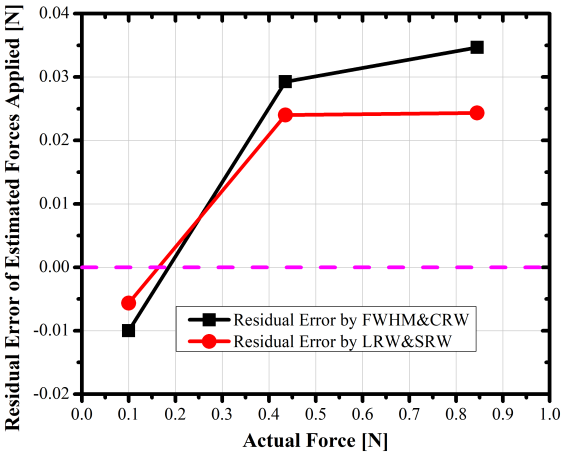

FIGURE 9. Residual error of both spectrum pairs in estimation of forces applied as a function of real ones.

estimation associated with RMSE of 1.08°C and 0.02 N only. Table 3 lists the main performance criteria of both methods.

As can be seen from the table the CFBG sensor module can distinguish between the two measurands accurately for both pairs. However, improvement in our temperature control system is required. For better comparison between the two pairs in terms of estimating the forces applied and

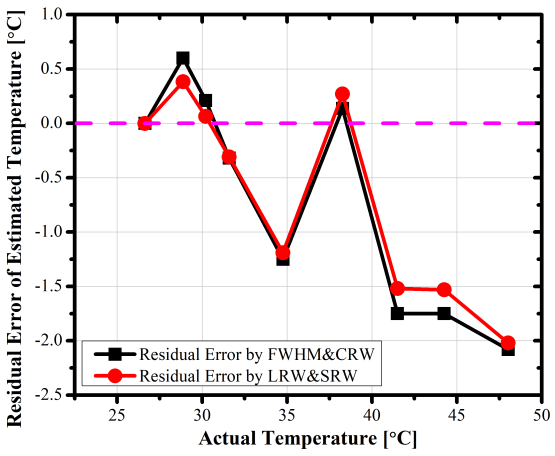

FIGURE 10. Residual error of both spectrum pairs in estimation temperature changes as a function of real value of temperature changes.

temperature changes, a plot of estimation's residual errors of both spectrum pairs as a function of real values are illustrated in Figure 9 and Figure 10. The horizontal pink line indicates the ideal sensor error in estimating the real values of the measurand. A reduction in the residual errors are clearly shown in Figure 9 for forces applied estimation by utilizing our proposed spectrum pair LRW&SRW, where the data are closer to the zero error than the data values of the other conventional pair FWHM&CRW. Same thing occurred in estimating the temperature changes, the LRW&SRW can provide better accuracy than the other pair except at ≈38°C where the FWHM&CRW has recorded less error.

IV. CONCLUSION

Discrimination between temperature and transverse forces is demonstrated experimentally in this work for the first time using two different interrogation methods of a single CFBG. A single CFBG was attached firmly to a flexible cantilever beam to create a simple CFBG sensor module. Two pairs of the CFBG's reflection spectrum have dual-parameter sensing ability to sense the forces and the temperature differently was investigated and compared. In this work, the sensing method in first pair was based on the conventional bandwidth tuning and center wavelength shift. However, there is no modification such as half-bonded CFBG or any other, it is instead simply bonded. While the sensing method in the second pair which is introduced by our group previously based on longer and shorter wavelength shifts. We have developed a linear model for both pairs to calculate the force and the temperature simultaneously. A series of experiments were carried out to calibrate, test repeatability, and validate measuring both the temperature and transverse forces in single measurement by both pairs. The results of the experiments show that the cantilever CFBG sensor module has a repeatability of 3.9 pm, 1.7 pm, 2.37 pm, 3.01 pm for FWHM&CRW and LRW&SRW pairs, respectively, and a high sensitivity of 48 pm/N, 286 – 336 pm/N for FWHM and wavelengths in response to applied forces. The sensor module also provides sufficient precision, with estimation errors for temperature and forces applied of only 1.08°C, 1.2°C, and 0.027 N, 0.02 N, respectively. It was revealed that the proposed pair LRW&SRW outperforms the conventional FWHM&CRW.

The significance of the proposed LRW&SRW which we will explore is that, if center wavelength combined with the two LRW&SRW, we believe in some configuration three physical quantities can be measured simultaneously using a single FBG.

REFERENCES

[1] M. M. Elgaud, M. S. D. Zan, A. G. Abushagur, A. A. A. Bakar, and A. M. Elshirkasi, "Analysis and simulation of time domain multiplexed (TDM) fiber Bragg sensing array using OptiSystem and OptiGrating," in *Proc. Int. Conf. Adv. Electr., Electron. Syst. Eng. (ICAEES)*, Nov. 2016, pp. 301–304, doi: 10.1109/ICAEES.2016.7888057.

[2] S. Sarkar, M. Tarhani, M. K. Eghbal, and M. Shadaram, "Discrimination between strain and temperature effects of a single fiber Bragg grating sensor using sidelobe power," *J. Appl. Phys.*, vol. 127, no. 11, Mar. 2020, Art. no. 114503, doi: 10.1063/1.5139041.

[3] P. Lu, L. Men, and Q. Chen, "Resolving cross sensitivity of fiber Bragg gratings with different polymeric coatings," *Appl. Phys. Lett.*, vol. 92, no. 17, May 2008, Art. no. 171112, doi: 10.1063/1.2919796.

[4] R. Aashia, K. V. Madhav, B. Srinivasan, and S. Asokan, "Strain-temperature discrimination using a single fiber Bragg grating," *IEEE Photon. Technol. Lett.*, vol. 22, no. 11, pp. 778–780, Jun. 1, 2010, doi: 10.1109/LPT.2010.2044657.

[5] A. Leal-Junior, A. Theodosiou, C. R. Diaz, C. Marques, M. J. Pontes, K. Kalli, and A. Frizera, "Simultaneous measurement of axial strain, bending and torsion with a single fiber Bragg grating in CYTOP fiber," *J. Lightw. Technol.*, vol. 37, no. 3, pp. 971–980, Feb. 1, 2019. [Online]. Available: http://jlt.osa.org/abstract.cfm?URI=jlt-37-3-971

[6] T. Guo, X. Qiao, Z. Jia, Q. Zhao, and X. Dong, "Simultaneous measurement of temperature and pressure by a single fiber Bragg grating with a broadened reflection spectrum," *Appl. Opt.*, vol. 45, no. 13, pp. 2935–2939, 2006, doi: 10.1364/AO.45.002935.

[7] T. Osuch, K. Markowski, and K. Jędrzejewski, "Numerical model of tapered fiber Bragg gratings for comprehensive analysis and optimization of their sensing and strain-induced tunable dispersion properties," *Appl. Opt.*, vol. 54, no. 17, p. 5525, Jun. 2015, doi: 10.1364/AO.54.005525.

[8] A. T. Augousti, *Fundamentals of Optical Waveguides*, vol. 15, no. 7, 2nd ed. Burlington, Vermont: Academic, 2006.

[9] A. A. G. Abushagur, N. Arsad, M. M. Elgaud, and A. A. A. Bakar, "Development of a 1-DOF force sensor prototype incorporating tapered fiber Bragg grating for microsurgical instruments," *IEEE Access*, vol. 7, pp. 168520–168526, 2019, doi: 10.1109/ACCESS.2019.2954914.

[10] K. Markowski, K. Jedrzejewski, and T. Osuch, "Numerical analysis of double chirp effect in tapered and linearly chirped fiber Bragg gratings," *Appl. Opt.*, vol. 55, no. 17, p. 4505, Jun. 2016, doi: 10.1364/AO.55.004505.

[11] T. Osuch, K. Markowski, and K. Jędrzejewski, "Fiber-optic strain sensors based on linearly chirped tapered fiber Bragg gratings with tailored intrinsic chirp," *IEEE Sensors J.*, vol. 16, no. 20, pp. 7508–7514, Oct. 2016, doi: 10.1109/JSEN.2016.2601332.

[12] A. A. G. Abushagur, N. Arsad, M. H. H. Mokhtar, and A. A. A. Bakar, "High sensitive microsurgical force sensor using spectral-width of tapered fiber Bragg gratings," in *Proc. IEEE Int. Conf. BioPhotonics (BioPhotonics)*, Sep. 2019, pp. 1–2, doi: 10.1109/BioPhotonics.2019.8896754.

[13] A. A. G. Abushagur, A. A. A. Bakar, and N. Arsad, "Development and preliminary data of integrated temperature-insensitive lateral force sensor based on linear chirp Fiber Bragg grating," *J. Phys. Conf. Ser.*, vol. 1371, Nov. 2019, Art. no. 12022, doi: 10.1088/1742-6596/1371/1/012022.

[14] A. A. G. Abushagur, N. Arsad, and A. A. A. Bakar, "Cantilever beam with a single fiber Bragg grating to measure temperature and transversal force simultaneously," *Sensors*, vol. 21, no. 6, p. 2002, Mar. 2021, doi: 10.3390/S21062002.

ABDULFATAH A. G. ABUSHAGUR received the B.E. degree in electrical engineering from the Higher Institute of Mechanical and Electrical Engineering, Houn, Libya, in 1992, and the M.Sc. degree in optical communication from Universiti Kebangsaan Malaysia (UKM), in 2012. He was with Photronix Technologies, Malaysia, designing/executing WDM couplers and optical splitters, from 2001 to 2005, and on development of fiber Bragg grating for filters/sensors, from 2005 to 2012, where he built a new automated FBG production line. He is currently working as a Senior Postdoctoral Researcher with UKM. His research interests include fiber Bragg grating sensors and its applications in biomedical engineering.

NORHANA ARSAD (Senior Member, IEEE) received the B.E. degree in computer and communication systems and the M.Sc. degree in photonics from Universiti Putra Malaysia (UPM), Malaysia, in 2000 and 2003, respectively, and the Ph.D. degree from the University of Strathclyde, Glasgow, U.K., in 2010. She is currently an Associate Professor with the Center of Advanced Electronic and Communication Engineering, Faculty of Engineering and Built Environment, Universiti Kebangsaan Malaysia. Her research interests include the investigation and design of fiber laser systems for application in spectroscopy, gas sensing, and photonics technology.

MOHAMED M. ELGAUD received the B.E. degree in electrical and electronic engineering from Benghazi University, Benghazi, Libya, in 2005, and the master's and Ph.D. degrees in electrical and electronic engineering from Universiti Kebangsaan Malaysia (UKM), Malaysia, in 2011 and 2019, respectively. He is currently a Joint Postdoctoral Researcher at the Photonics Technology Laboratory (PTL), Faculty of Engineering, UKM. His research interest includes the signal processing methods to improve distributed fiber optic sensors (DFOS).

AHMAD ASHRIF A. BAKAR (Senior Member, IEEE) received the bachelor's degree in electrical and electronics engineering from Universiti Tenaga Nasional, in 2002, the master's degree in communications and network system engineering from Universiti Putra Malaysia, in 2004, and the Ph.D. degree in electrical engineering from The University of Queensland, Australia, in 2010. He is actively involved in The Optical Society of America and Fiber Optic Association Inc., USA. He is devoting his research work on optical sensors in environmental and biomedical application, specifically in plasmonic waveguide sensor, polymeric electro-optic modulator waveguide, interferometer, evanescent field sensors, and devices based on nanoparticles and nanostructures.